Hepatocyte Versus Biliary Disease: A Distinction by Deconvolutional Analysis of Technetium-99m IDA Time-Activity Curves

Paul H. Brown, Jack E. Juni*, David A. Lieberman, Gerbail T. Krishnamurthy

Nuclear Medicine Service and Division of Gastroenterology, VA Medical Center and Departments of Diagnostic Radiology, Medicine, and Pathology, Oregon Health Sciences University, Portland, Oregon

A combination of quantitative hepatobiliary imaging techniques was developed to study normal control subjects and patients with 3 categories of hepatobiliary disease: 1) alcoholic cirrhosis; 2) sclerosing cholangitis; and 3) isolated common bile duct obstruction. Scintigraphic images were supplemented by quantitative measurement of hepatic extraction fraction by deconvolutional analysis and liver excretion $T_{½}$ by a nonlinear least squares method. In diseases confined primarily to the biliary tract (isolated common bile duct obstruction and sclerosing cholangitis), the mean hepatic extraction fraction as measured by deconvolutional analysis was not different from that in normal controls. In severe alcoholic cirrhosis, considered primarily a hepatocyte disease, the hepatic extraction fraction was markedly reduced. The $T_{½}$ excretion, compared to normal subjects, was prolonged in all three liver disease categories. We conclude that these quantitative parameters were able to detect hepatobiliary disease and to separate severe hepatocyte disease from biliary tract disease.

J Nucl Med 29:623–630, 1988

Imaging with technetium-99m analogs of iminodiacetic acid ([^{99m}Tc]IDA) has been shown to be useful in the diagnosis of various hepatobiliary diseases (*1*). The differentiation of primarily biliary from primarily hepatocyte disease by [^{99m}Tc]IDA imaging is not so straightforward. Several early studies differentiated hepatocyte from biliary disease based on a qualitative estimate of the degree of early hepatic uptake of the [^{99m}Tc]IDA (*2–4*). In primary biliary disease, the [^{99m}Tc]IDA agent is thought to be extracted rapidly from the blood by the hepatocyte and secreted into hepatic bile, but it may not be excreted into the intestine in presence of biliary obstruction. The result would be an image pattern of cholestasis, characterized by relatively good hepatic extraction from blood with retention of radiotracer in hepatic bile above the region of ductal obstruction. In hepatocyte disease, on the other hand, the hepatic extraction of the [^{99m}Tc]IDA from the blood is thought to be impaired, such that the [^{99m}Tc]IDA would remain in the blood pool for a longer period of time. In hepatocyte disease, this blood-pool activity within the liver results in an image pattern of nonspecific cholestasis. We investigated the usefulness of [^{99m}Tc]IDA imaging in distinguishing mild to severe hepatocyte disease from biliary disease in an objective fashion by employing deconvolutional analysis to measure hepatic extraction fraction, followed by a nonlinear least squares method for determination of liver excretion $T_{½}$. These methods are dependent on data already acquired as part of a standard [^{99m}Tc]IDA protocol in our department, so no additional data acquisition is needed.

MATERIALS AND METHODS

Four groups of subjects were studied: normal volunteer (control) subjects (n = 13), patients with isolated common bile duct obstruction (ICBDO, n = 14), sclerosing cholangitis (SC, n = 13), and alcoholic cirrhosis (n = 14). The ICBDO and SC patients had verification of their diagnosis by transhepatic or endoscopic retrograde cholangiography. The SC patients had involvement of both intra- and extrahepatic ducts and did not have evidence of portal hypertension (*5–7*). Patients with alcoholic cirrhosis had a compatible history of

Received Mar. 2, 1987; revision accepted Dec. 12, 1987.

For reprints contact: Paul H. Brown, Ph.D., VA Medical Center (115), PO Box 1034, Portland, OR 97207.

*Present address: University of Michigan Medical Center, Division of Nuclear Medicine, Ann Arbor, Michigan

alcohol intake and objective evidence of portal hypertension manifested by esophageal varices, or biopsy confirmed cirrhosis. The alcoholic cirrhosis patients were grouped by the Child-Turcotte classification as A, B, or C as shown in Table 1 (*8*). ICBDO and SC are considered to be primarily biliary diseases, at least early in the course of the disease, whereas alcoholic cirrhosis is primarily a hepatocyte disease.

All subjects fasted for at least 4 hr before receiving an intravenous (i.v.) injection of 3 mCi (110 MBq) of ^{99m}Tc-labeled diisopropyl iminodiacetic acid (Disofenin, DuPont Company, No. Billerica, MA). Planar data were recorded in a 64 × 64-byte mode (Medical Data Systems (Now MIPS), Ann Arbor, MI) computer matrix at one frame per minute, using a 15-inch field of view gamma camera with a low-energy general purpose collimator. Data analysis consisted of two methods: 1.) A deconvolution method to calculate the hepatic extraction fraction, and 2.) a nonlinear least squares method to measure excretion $T_{½}$.

Deconvolutional analysis (*9*) was performed using a right upper lobe liver time-activity curve as the output, with a heart curve as the input. The liver region of interest (ROI) was drawn (~50–100 pixels) carefully to include all of the right upper lobe while excluding any large ducts or scatter from the gallbladder. The heart ROI was drawn to include both the right and left ventricles. Care was exercised in drawing the liver and heart ROIs so as to avoid scatter from the heart into the liver and vice-versa. The study was reviewed in cine mode on the computer with the heart and liver ROIs displayed to insure adequate separation of the regions. The liver curve was smoothed before deconvolution. The liver true-response curve was deconvolved from the input and output curves using a Fourier transform technique with a smoothly decreasing long tail added to the end of the input and output curves (*10–11*). This long tail, in the shape of one-half of a cosine wave, avoids the high frequency artifacts caused by the precipitous fall in the time-activity curves at the end of the data acquisition period. The long added tail begins at the 30-min frame and falls to zero at the 128th added frame, giving the added tail a period of ~6 times the duration of acquisition. A tail with this length has been shown to be a minimum for avoiding high frequency artifact in the deconvolution process (*10*). The formula for the added tail in frame i of the heart or liver curve is given by:

$$TAIL = 0.5 \times AMP \times (\cos[\pi \times (i-30)/(128-30)] + 1),$$

where i = 30–128 and AMP is the heart or liver curve value (counts per pixel) at frame 30. The deconvolution is performed by obtaining the inverse Fourier transform of the quotient of the Fourier transforms of the output and input curves with the appended tails. The deconvolved true liver response curve, which includes the long appended tail, is then truncated to the time duration of the original study data.

TABLE 1
Child Classification of Cirrhosis*

Clinical/laboratory findings	Child Class A Minimal	B Moderate	C Advanced
Bilirubin mg%	< 2.0	2.0–3.0	> 3.0
Albumin mg%	< 3.5	3.0–3.5	> 3.0
Ascites	None	Controlled	Uncontrolled
Neurological disorder	None	Minimal	Advanced
Nutrition	Excellent	Good	Poor

*See Ref. *8*.

Deconvolution of data over the first 30 or 60 min produced similar results. In this investigation, our analysis utilized the first 30 min of data due to a restriction of the byte mode acquisition in the computer software. As the study progresses beyond 30 min, the gallbladder often accumulates a large number of counts/pixel, resulting in several overflows of the 64 × 64 8-bit byte mode. This is handled by the software by incrementing a scale factor and dividing the entire image matrix by 2. The end result, after 3–5 overflows, is a liver curve which spuriously shows a factor of 2 digital jumps back and forth between 16, 32, or 64 counts. Division by 2 at each overflow drops one bit of accuracy, and in the later frames of the study the statistical noise is amplified in the low-count density liver region. These artifacts cause difficulties in the least squares fit of the deconvolved curve. We chose to use frames 1–30 to avoid the low-count portion of the liver curve. On a system using word mode acquisition, a longer time interval could be used as desired, although 1–30 min is all that is needed. This problem is particular only to byte mode acquisition on the computer system.

The deconvolved liver curve represents a hypothetical true liver response curve, as if a perfect bolus injection had been made directly into the hepatic artery. If the hepatocytes are functioning normally, the amount of IDA extracted by the hepatocyte at any time is expected to be proportional to the amount of IDA in the blood, resulting in an exponentially decreasing response curve. In the case of poorly functioning hepatocytes, the hepatocytes cannot initially extract a proportionate amount of IDA from the blood, resulting in an initial peak on the response curve which becomes exponentially decreasing only in the later frames of the study (*11*). The hepatocyte extraction fraction (HEF) is the ratio of the (*Y*-intercept of the exponential fit) to the (maximum data point in the liver response curve) and represents a quantitation of the liver response curve as demonstrated in the following example:

$$\text{Hepatic Extraction Fraction (HEF)} = \frac{\text{Y intercept exponential fit liver response curve}}{\text{Y-MAX data value liver response curve}}.$$

The exponential fit is by linear least squares and includes those frames, working in reverse time order, from 30 min back to the first frame which visually departs significantly from the exponential fit. For normal hepatocytes, frames 30–1 will all lie on an exponential fitted curve as shown in the results section. For impaired hepatocytes, the fitted curve 30–1 will deviate markedly below the data points in the early frames, and the fit is repeated with these early points eliminated. Elimination of additional early points has little effect on the HEF. In this work, frames 30–1 were always fitted first and multiple other fits were evaluated visually if the frames 30–1 fit was unsatisfactory. The results section shows an example for alcoholic cirrhosis where frames 30–6 define the HEF. Basically, the later frames define an exponential clear-

ance which should extend all the way back to time zero. For normal hepatocytes, HEF = 100%; as liver function worsens the HEF will decrease as more of an "early overload of IDA peak" forms on the eventual exponential clearance curve. As part of an initial validation of our technique, the correspondence between HEF as measured here and the true physiologic extraction fraction in four pigs with liver transplant was established by dual isotope injection of [^{99m}Tc]IDA and [^{131}I] albumin in the hepatic artery and portal vein followed by sampling of the ^{99m}Tc to ^{131}I ratio in the inferior vena cava.

In addition to the HEF, the extraction $T_{½}$ of the fitted exponential deconvolved curve was also tabulated in each disease category.

The second method of data analysis, measurement of liver excretion $T_{½}$, was based on time-activity curves which were generated from the right upper lobe of the liver and the entire spleen after reviewing all 60 frames in a cine display. The spleen region was drawn carefully to avoid overlap of any intestinal activity in later frames of the study. The spleen time-activity curve, normalized to counts per pixel, was treated as a blood background and subtracted from the liver curve. The background corrected liver curve was modeled by an uptake-excretion compartmental model (*12*):

$$L(t) = k\,(e^{-0.693t/TE} - e^{0.693t/TU}),$$

where L(t) = background corrected liver cts/pixel at time t, k = a constant of the model, TE = excretion effective $T_{½}$, and TU = uptake effective $T_{½}$.

The best fit values of TE, TU and k were determined by a nonlinear least squares technique (*13*).

The spleen was chosen as the background organ based on our historical approach to this data analysis method. We began the least squares TU and TE analysis of the liver curve as our first approach, and this method failed to produce a good fit to the liver data points unless a background organ was subtracted from the liver. Use of the heart, the logical choice, as a background organ results in negative data values in the first few minutes of the study, evidently because the heart contains more blood counts than does the liver. Negative data values are not physiologically possible. Since the spleen and liver share a common arterial blood supply, we tried the spleen as a blood background and found, empirically, that it allowed a good least squares fit to the data points without producing any oversubtraction problems. Of course, the true mathematical answer to removing blood background is a convolution between the input (heart) and liver, which we began as a method of analysis only after we discovered that the least squares technique did not appear to be distinguishing between the various disease states.

RESULTS

Figure 1 shows the distribution of HEF for the four disease categories. Figure 2 shows the HEF data and fitted line for a typical normal subject. The exponential fit for the HEF in Figure 2 is for all data points in the

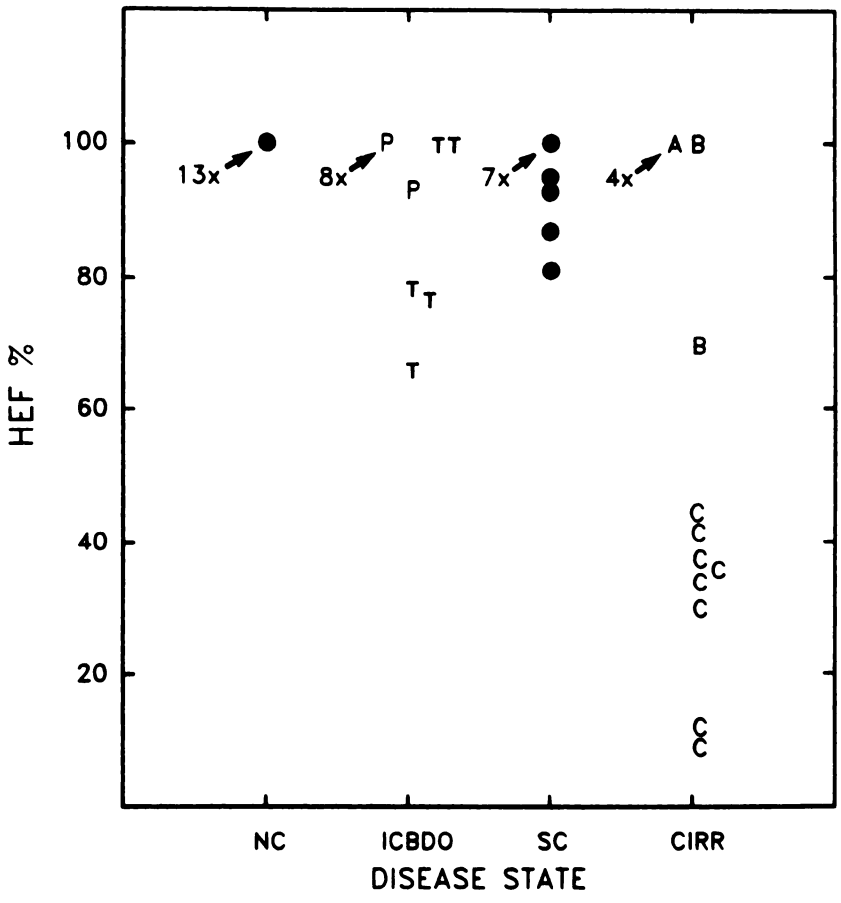

FIGURE 1
Hepatocyte Extraction Fraction for normal controls (NC), isolated common bile duct obstruction (ICBDO), sclerosing cholangitis (SC), and alcoholic cirrhosis (CIRR). For ICBDO a P denotes partial obstruction and a T denotes total obstruction. For CIRR, Child classification is A (mild), B (moderate), or C (severe).

range 1–30 min. The HEF for this normal control is 100% since the ratio of the *Y*-intercept of the fitted curve to the peak data point is 1:1. The HEF in the two biliary diseases (ICBDO and SC) is shown for typical subjects in Figures 3 and 4, respectively. The HEF remains near 100% in these biliary diseases and was not different from that in normal controls using analysis of variance (ANOVA) with a Newman Keuls test (see Table 2).

The HEF in a typical Class C alcoholic cirrhosis patient is shown in Figure 5. The HEF of 38% in Figure 5 was derived from the fitted exponential line, with the fit range beginning at the last data point and extending back towards t = 0 until the fitted exponential line deviated markedly from the data points. In Figure 5, the fitted range was 30–6 min. This then defines the *Y*-intercept of the fit, which is 38% of the maximum data point at t = 1 min. The mean HEF for the alcoholic

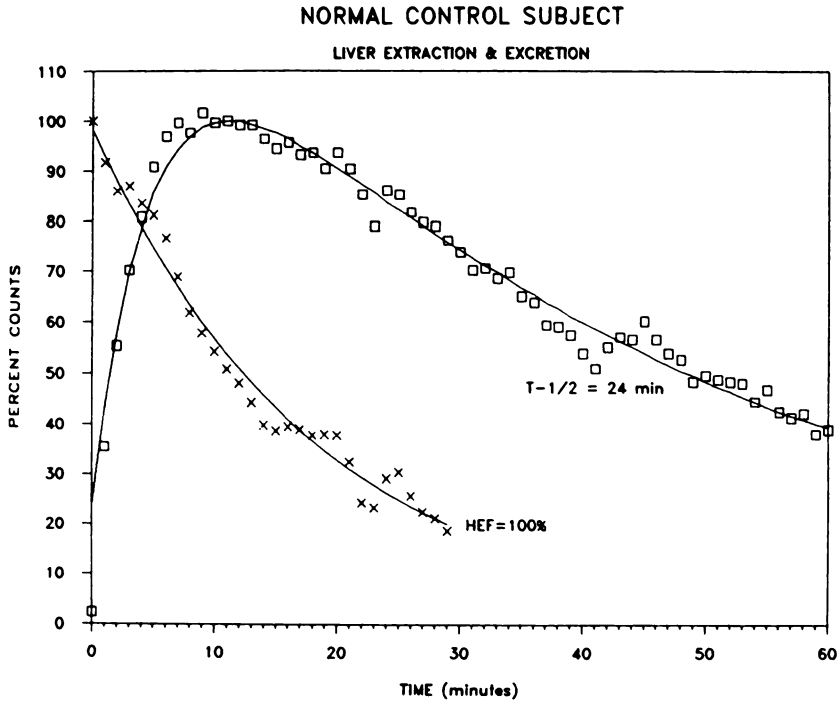

FIGURE 2
Normal control subject liver extraction and excretion. The *X* data points from 1–30 min are the deconvolved extraction data with the exponential fitted curve defining the hepatocyte extraction fraction (HEF) as noted on the figure. The square data points from 1–60 min represent the background corrected liver counts, normalized to 100% at the maximum. The fitted line 1–60 min is the two-compartment excretion model with an excretion $T_{½}$ as noted on the figure.

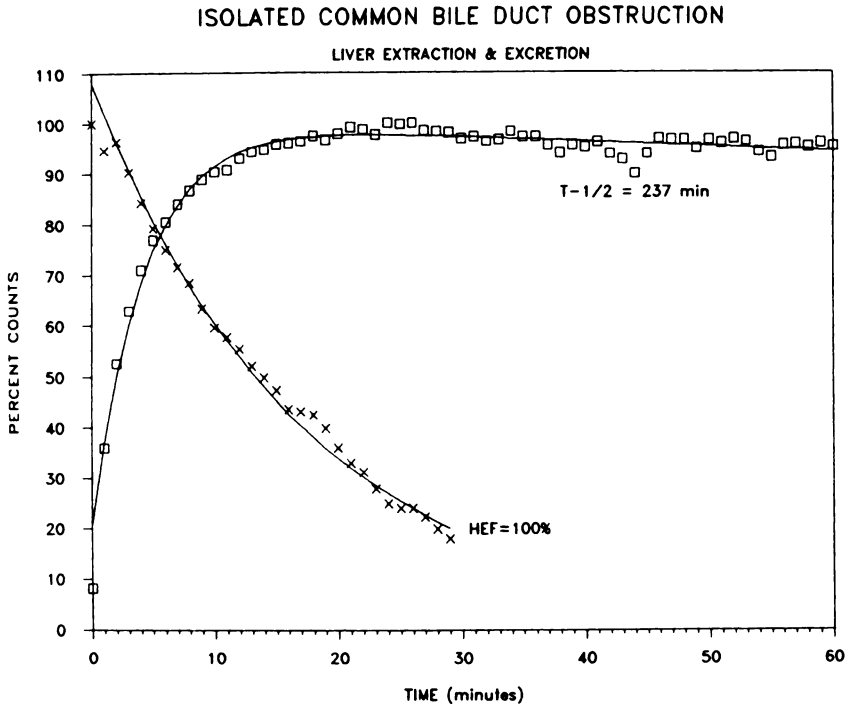

FIGURE 3
Same data in Figure 2 for isolated common bile duct obstruction.

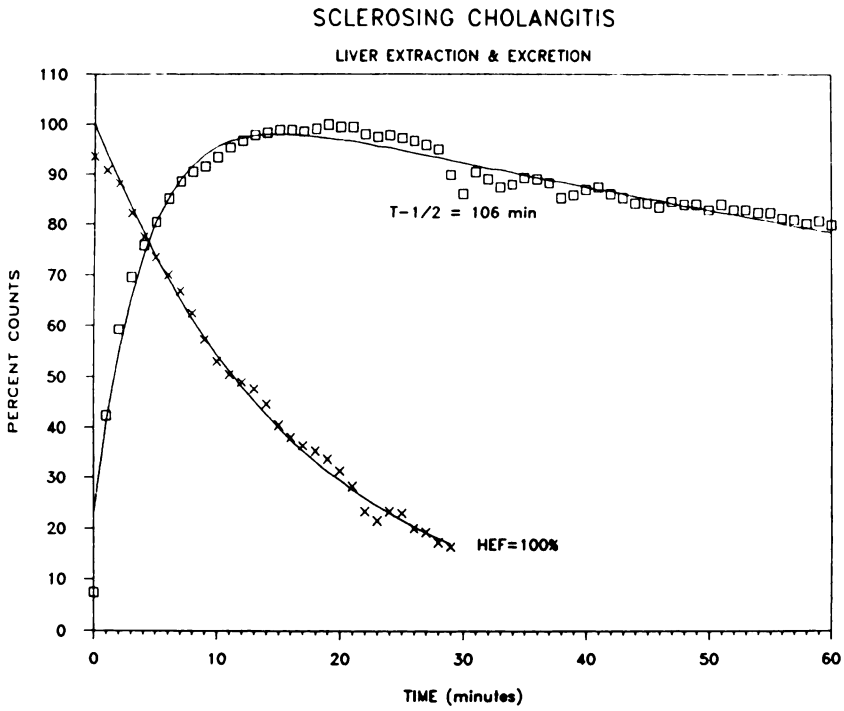

FIGURE 4
Same data in Figure 2 for sclerosing cholangitis.

TABLE 2
IDA Liver Test Parameters for Various Disease States (Mean ± s.e.)

Group	Hepatocyte extraction fraction (%)	Effective excretion $T_{½}$ (min)
Normal (n = 13)	100 ± 0	19 ± 1*
CBD Obstruction (n = 14)	94 ± 3	90 ± 25
SC (n = 13)	96 ± 2	85 ± 11
Alcoholic cirrhosis (n = 14)	60 ± 9**	70 ± 14
Child Class A (n = 4)	100 ± 0	46 ± 9
Child Class B (n = 2)	86 ± 15	73 ± 33
Child Class C (n = 8)	32 ± 5***	81 ± 23

* Different from the other groups at $p < 0.005$ by ANOVA.
** Different from the other groups at $p < 0.001$ by ANOVA.
*** Different from the other Child classes at $p < 0.001$ by ANOVA.

cirrhosis patients was significantly lower than the other subject groups at $p < 0.001$ by ANOVA (see Table 2).

The result of the HEF verification by arterial/venous dual isotope counting in the four transplant pigs was that both the [^{99m}Tc]IDA deconvolutional HEF and the measured arterial/venous extraction fraction were measured to be 100%. The verification must be considered as a work-in-progress, with further studies needed on animals with lower values of HEF. These results do, however, provide an indication that the [^{99m}Tc]IDA HEF is truly measuring the physiological extraction fraction.

The extraction $T_{½}$ mean ± s.e.m. of the fitted deconvolved curves was 10 ± 1, 13 ± 2, 14 ± 2, and 14 ± 2 minutes in the normals, ICBDO, SC and cirrhosis, respectively. These deconvolved extraction $T_{½}$ were not statistically different ($p = 0.13$). The extraction $T_{½}$ of the deconvolved curve was thus not useful in defining the disease state.

Figure 6 shows the distribution of excretion $T_{½}$ for the four disease categories. Figure 2 shows excretion data points from a normal control with the compartmental model fitted line for excretion $T_{½}$ equal to 24 min. Figures 3, 4, and 5 show excretion curves for ICBDO, SC, and alcoholic cirrhosis, respectively. Note that while the disease etiology is different in Figures 3 and 5, obstruction versus cirrhosis, the excretion was prolonged in a similar fashion in both diseases ($T_{½}$ = 237 and 232 min). Table 2 shows that all three disease categories had a mean excretion $T_{½}$, which was significantly higher than the normal controls ($p < 0.005$). There were no significant differences in $T_{½}$ between ICBDO, SC, or alcoholic cirrhosis. Five of our patients (4 ICBDO and 1 SC) had a liver time-activity curve that continued to have increasing counts through the entire 60-min study. These patients were excluded from the statistical comparisons between groups of subjects and a value of infinity was assigned to their excretion half-life, indicating that the model could not accurately measure their greatly prolonged excretion half-life.

Another interesting result was obtained when the 14 alcoholic cirrhosis patients were grouped by Child classification (*8*). Table 2 shows that the HEF for Class C subjects was reduced compared to Class A and B subjects. The Class A and B subjects had HEF, which was

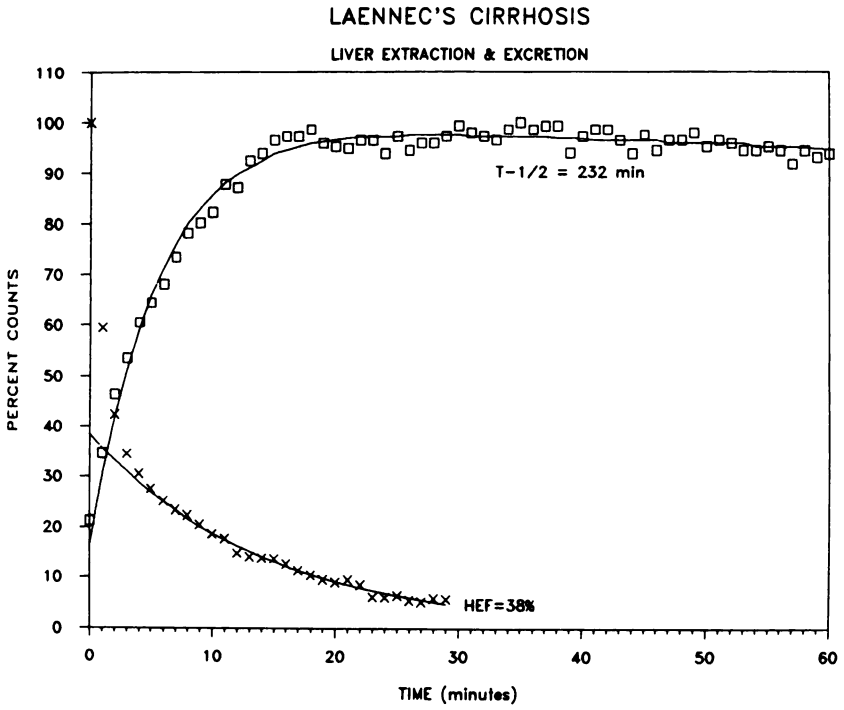

FIGURE 5
Same data in Figure 2 for alcoholic (Laennec's) cirrhosis.

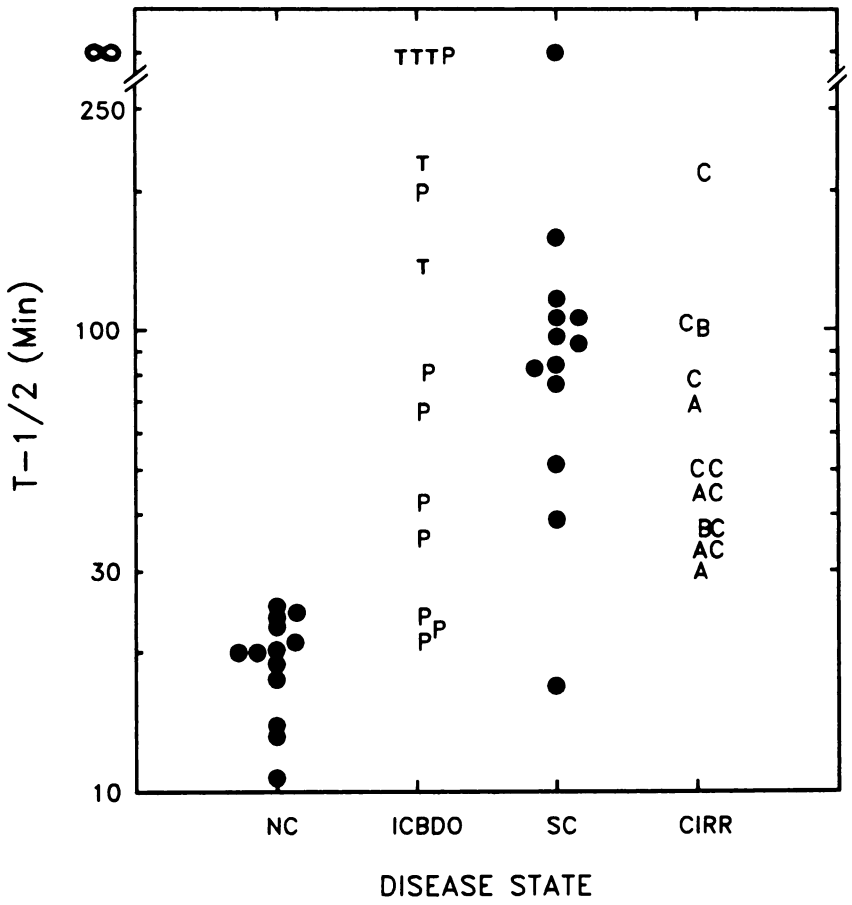

FIGURE 6
Excretion $T_{½}$ for normal controls (NC), isolated common bile duct obstruction (ICBDO), sclerosing cholangitis (SC), and alcoholic cirrhosis (CIRR). For ICBDO, a P denotes partial obstruction and a T denotes total obstruction. For CIRR, Child classification is A (mild), B (moderate), or C (severe).

not different from normal or biliary disease subjects (HEF = 100%). There were no statistical differences between the three cirrhosis classes in their excretion $T_{½}$ (see Table 2).

The ICBDO patients were similarly classified based on their cholangiography as complete (n = 5) or partial (n = 9) obstruction. The complete obstruction HEF mean was 84 ± 7, compared to 99 ± 1 in partial

obstruction ($p = 0.01$), suggesting that complete obstruction may impair hepatocyte function.

The uptake $T_{½}$ (TU) in the liver least squares model was not different in the four disease states (3.5 ± 0.6, 5.9 ± 2.0, 4.9 ± 0.6, 6.5 ± 1.6 min, $p = 0.47$ by ANOVA). Thus, although both the uptake TU and excretion TE are necessary to produce a good fit to the liver data points, only the excretion TE appears to have a clinical utility. The TU value was nominally a factor of 10 smaller than the TE, indicating that the TU would only have a strong effect on the early frames of the liver clearance curve.

DISCUSSION

Our previous studies have shown that the hepatobiliary image pattern permits some discrimination between intrahepatic and extrahepatic diseases, especially when combined with ultrasound (*14*). In this investigation, we have employed deconvolutional analysis, which appears to increase the sensitivity for separating primarily hepatocellular disease from primarily biliary disease (*10–11*), especially in early biliary disease. If secondary biliary cirrhosis results from chronic biliary disease, the hepatic function may also be impaired, and the HEF lowered. The early nature of disease in our SC patients was suggested by their lack of portal hypertension or any other signs of cirrhosis of the liver.

Mathematically, the observed liver radioactivity at any time is a convolution of the true liver counts with the blood counts for all preceding time. Deconvolution attempts to derive the true liver counts from the observed liver counts, when the observed liver counts are masked by recirculation of the [^{99m}Tc]IDA within the liver blood pool. An alternative viewpoint is to simply consider that the deconvolved liver curve is the time-activity curve that would be obtained with a perfect, infinitesimally short, bolus injection directly into the hepatic artery, with no recirculation of the tracer. A detailed description of deconvolutional analysis is available elsewhere as applied to nuclear nephrology (*15*). Once the deconvolutional analysis is completed, it is still necessary to derive some quantitative parameters that describe the liver response curve. We observed that primarily hepatocyte disease resulted in an early peak on the liver response curve which appeared to be superimposed on an exponential clearance curve. This early peak on the liver response curve was quantified by the HEF. In preliminary animal experiments, we have shown that the HEF agreed with measurement of the physiologic extraction fraction by arterial/venous sampling.

The HEF was not different from the normal value of 100% in biliary diseases (ICBDO, SC) as shown in Table 2 and Figure 1. This normal HEF, in the presence of ductal disease, is interpreted as a reflection of normally functioning hepatocytes. As noted below, the excretion $T_{½}$, on the other hand, was prolonged in biliary disease. The mean HEF was reduced in severe hepatocyte disease (alcoholic cirrhosis) as shown in Table 2 and Figure 1. The reduced HEF in hepatocyte disease, shown in Figure 5, is caused by the early peak on the liver response curve. We interpret this peak as an early overload of IDA, or as the inability of the hepatocyte to extract IDA from the blood in proportion to the amount of IDA present, which would lead to an exponentially decreasing curve. Eventually the hepatocyte does manage to begin exponential extraction of IDA as shown by the later portion of Figure 5. The rate of this extraction (deconvoluted extraction $T_{½}$) was not statistically different in the four disease categories. When the severity of alcoholic cirrhosis was categorized by Child classification (*8*), it was found that Class A and B cirrhotics had normal HEF, whereas Class C cirrhotics had markedly reduced HEF as shown in Table 2 and Figure 1. These data suggest that HEF may be a measure of liver function or a measure of liver reserve that could provide useful information to the gastroenterologist and surgeon. Further studies in an animal model with progressive liver damage may be necessary to further define the role of deconvolutional HEF in the failing liver. HEF has been used to serially monitor liver transplants (*16*) where it was found that HEF changes preceded bilirubin increases. The Fourier transform with the long appended tail method of deconvolution has been verified in an in vitro model of hepatic blood flow (*17*) for determination of hepatic artery/portal vein perfusion.

Our results (Figs. 2–5) show that a two-compartment model of uptake-excretion (*12*) produces fitted time-activity curves that agree closely with the actual patient data points in normal subjects, ICBDO, SC and alcoholic cirrhosis, similar to observations made by others (*18–19*). The excretion $T_{½}$ was prolonged similarly in both hepatocyte (alcoholic cirrhosis) and biliary diseases (SC and ICBDO) (see Fig. 6). This prolonged excretion $T_{½}$ is a reflection of cholestasis either at the ductal or canalicular level in ICBDO or SC (*20–21*), or cholestasis at the hepatocyte level in alcoholic cirrhosis. We have previously shown that liver excretion $T_{½}$ is nonspecific and correlates with the severity of disease irrespective of its etiology (*14*).

The quantitative evaluation of liver time-activity curves is a quick and simple means for detecting the presence of disease and also for classifying the disease as primarily severe hepatocyte or primarily biliary. Combining the quantitative curve analysis with the image pattern allows specification of a wide variety of diseases, including isolated common bile duct obstruction (*1*), sclerosing cholangitis, primary biliary cirrhosis (*22–23*), and severe alcoholic cirrhosis.

ACKNOWLEDGMENT

This research was supported by the Veterans Administration.

REFERENCES

1. Weissmann HS, Freeman LM. The biliary tract. In: *Freeman and Johnson's clinical radionuclide imaging*, Vol. 2, 3rd Ed. Orlando: Grune and Stratton, 1984:879–1050.
2. Pauwels S, Steels M, Piret L, et al. Clinical evaluation of Tc-99m-diethyl-IDA in hepatobiliary disorders. *J Nucl Med* 1978; 19:783–788.
3. Pauwels S, Piret L, Schoutens A, et al. Tc-99m-diethyl-IDA imaging: Clinical evaluation in jaundiced patients. *J Nucl Med* 1980; 21:1022–1028.
4. Kim EE, Domstad PA, Choy YC, et al. Complementary role of reticuloendothelial and hepatobiliary imaging agents in assessment of liver disease. *Clin Nucl Med* 1982; 7:64–66.
5. Wiesner RH, LaRusso NF, Ludwig J, et al. Comparison of the clinicopathologic features of primary sclerosing cholangitis and primary biliary cirrhosis. *Gastroenterology* 1985; 88:108–114.
6. Wiesner RH, Ludwig J, LaRusso NF, et al. Diagnosis and treatment of primary sclerosing cholangitis. *Sem Liver Dis* 1985; 5:241–253.
7. LaRusso NF, Wiesner RH, Ludwig J, et al. Current concepts primary sclerosing cholangitis. *N Engl J Med* 1986; 310:899–903.
8. Child III CG, Turcotte JC. Surgery and portal hypertension. In: Child III CG, ed. *The liver and portal hypertension.* Philadelphia: W.B. Saunders, 1964:50
9. Williams DL. Improvement in quantitative data analyses by numerical deconvolution techniques. *J Nucl Med* 1979; 20:568–569.
10. Juni JE, Thrall JH, Froelich J, et al. A simple technique for reducing deconvolution artifact in scintigraphic studies. In: *Proceedings Medcomp '82—First IEEE Computer Society International Conference on Medical Computer Science/Computational Medicine.* Piscataway, NJ: IEEE, 1982:174–177.
11. Juni JE, Keyes JW, Carter W, et al. Differentiation of obstructive from nonobstructive jaundice by deconvolutional analysis of hepatobiliary scans. *J Nucl Med* 1983; 24:P30.
12. Brown PH, Krishnamurthy GT, Bobba VR, et al. Radiation dose calculation for Tc-99m HIDA in health and disease. *J Nucl Med* 1981; 22:177–181.
13. Bevington PR. *Data Reduction and Error Analysis for the Physical Sciences.* New York: McGraw Hill, 1969:204–246.
14. Lieberman DA, Krishnamurthy GT. Intrahepatic versus extrahepatic cholestasis discrimination with biliary scintigraphy combined with ultrasound. *Gastroenterology* 1986; 90:734–743.
15. O'Reilly PH, Shields RA, Testa HJ. *Nuclear Medicine in Urology and Nephrology.* London: Butterworth, 1979:168–176.
16. Reichle R, Campbell D, Tagge E, et al. Quantitative assessment of liver transplant function by deconvolutional analysis. *J Nucl Med* 1986; 27:1013.
17. Juni JE, Reichle R, Pitt S, et al. Quantitative measurement of hepatic artery and portal vein blood flow by deconvolutional analysis. *J Nucl Med* 1986; 27:957.
18. Velchik MG, Schwartz W, London JW, et al. Quantitative analysis of liver function in percutaneous transhepatic biliary drainage patients. *Clin Nucl Med* 1985; 10:80–35.
19. Gelius L, Skretting A, Aas M. A mathematical model for liver uptake and excretion of 99m-Tc diethyl IDA. *Eur J Nucl Med* 1981; 6:139–142.
20. Ament AE, Bick RJ, Miraldi FD, et al. Sclerosing cholangitis: Cholescintigraphy with Tc-99m labeled DISIDA. *Radiology* 1984; 151:197–201.
21. May GR, Bender CE, LaRusso NF, et al. Nonoperative dilatation of dominant strictures in primary sclerosing cholangitis. *Am J Roentgenol* 1985; 145:1061–1064.
22. Krishnamurthy S, Krishnamurthy GT, Keeffe EB, et al. Differentiation of primary sclerosing cholangitis from primary biliary cirrhosis by Tc-99m-IDA scintigraphy. *J Nucl Med* 1986; 27:1012.
23. Rodman CA, Keeffe EB, Lieberman DA, et al. Diagnosis of sclerosing cholangitis with Tc-99m-labeled iminodiacetic acid planar and single photon emission computed tomographic scintigraphy. *Gastroenterology* 1987; 92:777–785.